



RESEARCH ARTICLE

10.1029/2024GC011522

Key Points:

- We show quantitatively (via analysis of variance) that a non-random process controls the relationship between He (>0.3%) and both basement faults and intrusions
- Strong correlations of He wells to both basement faults and intrusions suggest that advective transport via faults/intrusions facilitates He migration
- We present a predictive exploration model (intersection of basement faults and intrusions) that can be translated to other areas to generate He prospects

Supporting Information:

Supporting Information may be found in the online version of this article.

Correspondence to:

D. T. Halford,
d.t.halford@gmail.com

Citation:

Halford, D. T., Karolytė, R., Andreason, M. W., Cathey, B., Cathey, M., Dellenbach, J. T., et al. (2024). Probabilistic determination of the role of faults and intrusions in helium-rich gas fields formation. *Geochemistry, Geophysics, Geosystems*, 25, e2024GC011522. <https://doi.org/10.1029/2024GC011522>

Received 21 FEB 2024

Accepted 5 JUN 2024

Author Contributions:

Conceptualization: D. T. Halford, R. Karolytė, C. J. Ballentine

Formal analysis: D. T. Halford, R. Karolytė, M. W. Andreason, B. Cathey, M. Cathey, J. T. Dellenbach, J. J. Cuzella, A. Cheng, K. J. W. McCaffrey, J. G. Gluyas, C. J. Ballentine

Methodology: D. T. Halford, R. Karolytė, M. W. Andreason, B. Cathey, M. Cathey, J. T. Dellenbach, J. J. Cuzella, A. Cheng,

Probabilistic Determination of the Role of Faults and Intrusions in Helium-Rich Gas Fields Formation

D. T. Halford¹ , R. Karolytė¹ , M. W. Andreason², B. Cathey³, M. Cathey³, J. T. Dellenbach⁴ , J. J. Cuzella⁴ , S. A. Sonnenberg⁵ , A. Cheng¹ , K. J. W. McCaffrey⁶ , J. G. Gluyas⁶ , and C. J. Ballentine¹

¹Earth Sciences, University of Oxford, Oxford, UK, ²Navajo Nation Oil and Gas Company, St. Michaels, AZ, USA,

³Earthfield Technology LLC, Richmond, TX, USA, ⁴Division of Energy and Mineral Development, Lakewood, CO, USA,

⁵Colorado School of Mines, Geology & Geological Engineering, Golden, CO, USA, ⁶Earth Sciences, Durham University, Durham, UK

Abstract Natural gas fields with economic helium (>0.3 He %) require the radioactive decay of crustal uranium (U) and thorium (Th) to generate He and tectonic/structural regimes favorable to releasing and concentrating He. An unknown is determining the role of faults and structural features in focusing deep-seated He sources on shallow accumulations. We tested the correlation between high-He wells ($n = 94$) and structural features using a new high-resolution aeromagnetic survey in the Four Corners area, USA. A depth-to-basement map with basement lineaments/faults, an intrusion map, and a flattened basement structural high map were created using Werner deconvolution algorithms by combining magnetic, gravity, and topography data with magnetic and gravity depth profiles. We show quantitatively (via analysis of variance) that a non-random process controls the relationship between He (>0.3%) and both basement faults and intrusions: 88% of high-He wells occur <1 km of basement faults; and 85% of high-He wells occur <1 km of intrusions. As He % increases, the distance to the structural features decreases. Strong spatial/statistical correlations of He wells to both basement faults and intrusions suggest that advective transport via faults/intrusions facilitates He migration. The role of gas phase buoyancy and structural trapping is confirmed: 88% of high-He occurs within basement structural highs, and 91% of the remaining wells are <1 km from intrusions (potential structural high). We present a composite figure to illustrate how a probabilistic approach can be used as a predictive model to improve He exploration success by targeting zones of intersection of basement faults and intrusions within basement structural highs.

Plain Language Summary Helium, which is a colorless and odorless gas, is an important and irreplaceable commodity that is used in a variety of modern applications. Helium is often found comingled with natural gases in underground rocks. The exact importance of structural features in the accumulation of significant amounts of helium underground is largely unknown. In this study, we utilize high resolution geophysical techniques focused in the Four Corners Area, USA combined with geochemical data of helium sampled from oil/gas wells to investigate the role of structural features on helium's occurrence. We show that helium occurrences are not randomly related to structural features (basement faults and/or intrusions) using statistical tests. In fact, we show that helium percentages in natural gas increase as one moves closer to basement faults and/or intrusions. Furthermore, we suggest that these faults and intrusions likely help enable helium gas migration from deeper areas to shallower areas underground based on the strong spatial and statistical correlations of helium wells to basement faults and intrusions. We also construct a predictive composite figure using structural elements that are likely favorable to helium accumulation to aid in exploring new areas of undiscovered helium gas accumulations in the subsurface.

1. Introduction

Helium (He), a natural resource derived from the radioactive decay of subsurface uranium (U) and thorium (Th), is irreplaceable in medical applications, low-carbon technologies, science and engineering, nuclear power, and the aerospace industry (e.g., Anderson, 2018; Boreham et al., 2018; National Research Council, 2010). The Four Corners area, USA, has natural gas with high He (>10%) in some areas (Brennan et al., 2021; Casey, 1983). Originally, He was discovered serendipitously through hydrocarbon exploration, but now He is a primary exploration target (Cheng et al., 2023; Danabalan et al., 2022). The shift of He to a primary exploration target is crucial to support He's increased global demand and dwindling supply (Olafsdottir & Sverdrup, 2020).

K. J. W. McCaffrey, J. G. Gluyas,
C. J. Ballentine

Supervision: R. Karolytė, C. J. Ballentine

Visualization: D. T. Halford,

M. W. Andreason, B. Cathey, M. Cathey

Writing – original draft: D. T. Halford

Writing – review & editing:

D. T. Halford, R. Karolytė,

M. W. Andreason, B. Cathey,

J. T. Dellenbach, J. J. Cuzella,

S. A. Sonnenberg, K. J. W. McCaffrey,

J. G. Gluyas, C. J. Ballentine

The helium system is defined as any subsurface natural gas system, and its associated geological processes and elements that allow the accumulation of economic levels of He ($>0.3\%$ for direct and secondary extraction, $>0.04\%$ for liquefied natural gas operations) in the gas stream beyond the ubiquitous trace amounts found within Earth's mantle, atmosphere, hydrosphere, and crustal sources (Boreham et al., 2018; Danabalan et al., 2022; Halford, 2018; Halford et al., 2022). In order to establish a significant He reservoir, there are several major variables that must be considered: (a) source rocks, (b) heating and fluid interactions, (c) migration pathways, (d) seals/traps, and (e) time (Boreham et al., 2018; Cheng et al., 2021, 2023; Danabalan et al., 2022; Halford, 2018; Halford et al., 2022; Karolytė et al., 2022). The role of regional heat flow and tectonics in enhancing helium release from regional sources has been established (Danabalan et al., 2022; Lowenstern et al., 2014; Torgersen, 2010) and we focus here on developing our understanding of the transport pathways.

In the Four Corners area, He discoveries ($n = 94$) are often near structural features (i.e., Precambrian basement sutures or mapped surface traces of structures) (Craddock et al., 2017; Halford et al., 2022). Previous work observed little variance in $^4\text{He}/\text{N}_2$ in the Four Corners gas fields to argue for fault controlled advective free-gas He migration from the crystalline basement to trapping structures (Halford et al., 2022). While high-He gas has been postulated to be correlated with structural features, such as faults and intrusions (Boles et al., 2015; Buttitta et al., 2020; Craddock et al., 2017; Danabalan et al., 2022; Halford et al., 2022; Karolytė et al., 2022; Mtili et al., 2021; Tardani et al., 2016) the data, until now, to quantifiably test this concept for high-He gas field formation, has not been available. Using newly acquired high-resolution geophysical data (Figure 1) combined with geochemical data sets within the Four Corners area, we test the hypothesis that faults and intrusions are spatially correlated with high He, which may be translated to regions outside the Four Corners area. By comparing observed He occurrences and synthetic data sets of randomly located points to investigate the spatial relationship to structural features, we find their relative density distributions are statistically distinct, suggesting a non-random and helium specific process is controlling their relationship.

2. Geologic Background

The Four Corner's area of the USA, where the states of Colorado, New Mexico, Utah and Arizona converge, has experienced a complex geologic history pertaining to basement features and igneous activity. The larger Southern Rocky Mountain region, which includes the Four Corners area, records lithospheric assembly during the Paleo-Proterozoic time (1.8–1.6 Ga), intracratonic magmatism during the Meso-Proterozoic (1.44–1.35 Ga), incipient rifting (1.1–0.5 Ga), ancestral Rocky Mountain development during the Paleozoic (350–290 Ma), Laramide tectonism during the Cretaceous-Paleogene (75–45 Ma), and Paleogene-Neogene extension, magmatism, and uplift (Gilfillan et al., 2008; Karlstrom & Humphreys, 1998).

The heterogeneous Paleoproterozoic and Mesoproterozoic crystalline basement underlying the Colorado Plateau contains numerous basement suture zones, which are commonly marked by diffuse fault systems and/or discrete shear zones (Craddock et al., 2017; Davis & Bump, 2009). Master shear zones are rooted in the deep seated zones of weakness within the basement and most are presumably originating along reactivated deep-seated Neoproterozoic shear zones (Davis & Bump, 2009; Whitmeyer & Karlstrom, 2007). Thus, suture zones and shear zones represent deformational boundaries that define the underlying Paleoproterozoic basement provinces in the area (Mojave, Yavapai and Mazatzal) (Karlstrom & Humphreys, 1998).

The field area within the Four Corners region consists of intrusive plutons, and Paleogene-Neogene mafic and ultra-mafic diatremes and lamprophyres that were emplaced along structurally weak crustal extension zones (Gonzales & Lake, 2017; Re et al., 2015). Dikes and sills related to these diatremes and intrusive bodies intersect and crosscut the sedimentary section (Danie, 1978; Masters, 2000). More specifically, the Navajo Volcanic Field (NVF), which results from slab rollback of the Farallon plate (Gonzales & Lake, 2017; Hernández-Urbe & Palin, 2019), exists within the study area and comprises >80 mafic and ultra-mafic diatremes of Oligocene to Miocene age (28–19 Ma) and hundreds of intrusive plutons (Bélanger & Ross, 2018; Semken, 2003). Despite the volcanos of the NVF not being located along exposed faults, the magma ascent was likely aided by fractures at depth (Delaney, 1987).

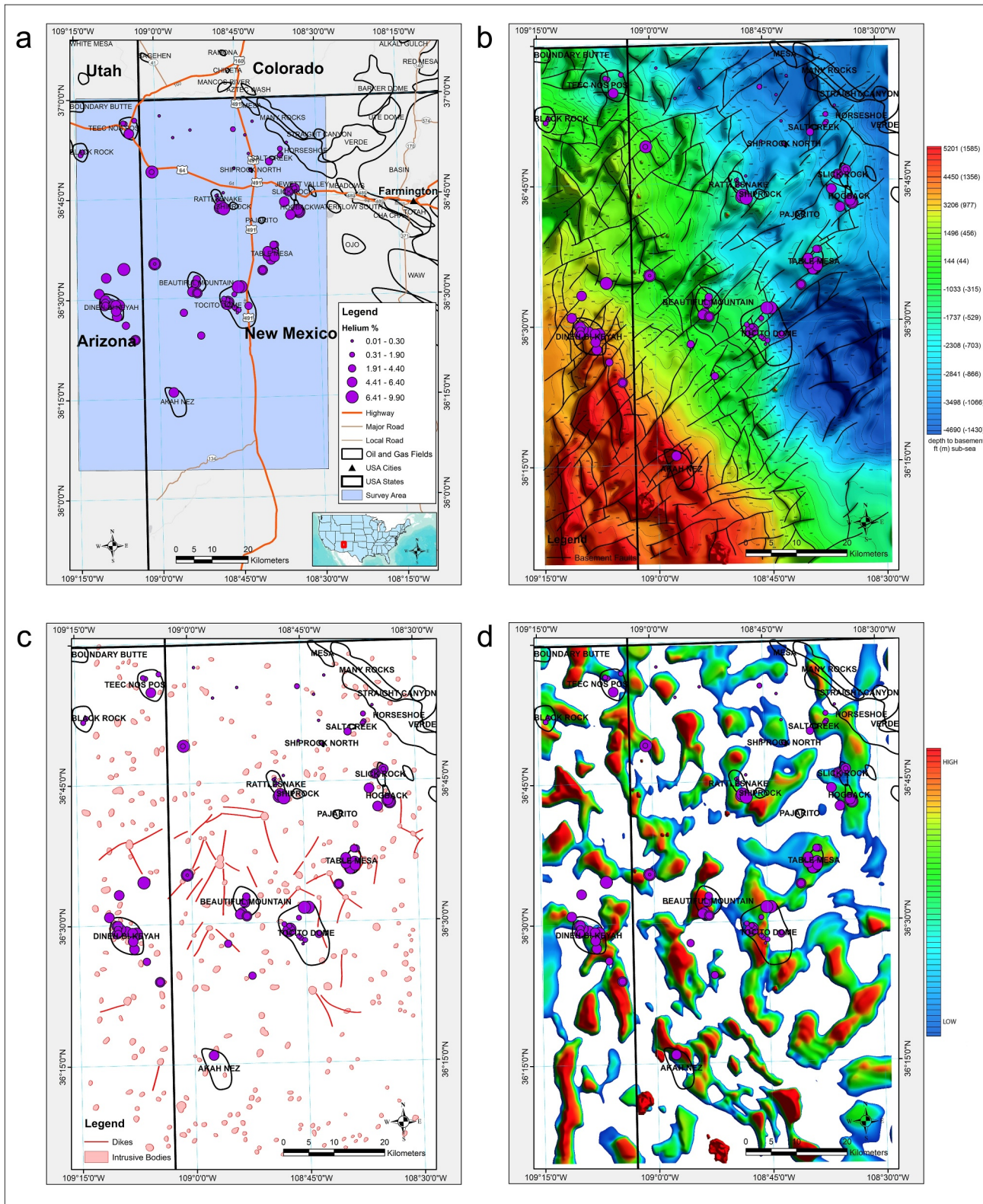


Figure 1. (a) Location map with the study area (blue rectangle). Maps calculated from the high-resolution geophysical data (mod. from Andreason et al., 2022): (b) Depth-to-basement map with interpreted basement faults/lineaments as black lines, (c) intrusions (red polygons) and dikes (red lines) map, (d) localized basement structure map from flattened depth-to-basement map illustrates structural highs with an arbitrary scale from red (high) to blue (low). He molar % is overlain on all maps as purple circles (Brennan et al., 2021; Halford et al., 2022).

3. Methodology

3.1. Aeromagnetic Geophysical Data Collection

Aeromagnetic geophysical data was acquired by Earthfield Technology on behalf of the Navajo Nation Oil and Gas Company in 2021 using an airborne magnetometer, which measures and records the total magnetic field (Andreason et al., 2022). By flying a Cessna C-180 aircraft at 152 m with a fitted tail-stinger which housed a Geometrics G823A Cesium-vapor Magnetometer System, 20,761-line km of high-resolution aeromagnetic data were collected. Flight lines and tie lines were spaced 400 and 1,600 m, respectively. Ancillary airborne equipment and a ground-based magnetometer were also utilized (Andreason et al., 2022).

3.2. Geophysical Pre-Processing

Quality control checks were completed prior to the profile data processing and leveling procedures by Earthfield Technology (Andreason et al., 2022). Pre-processing procedures include the following listed below:

Data Merging: Data traces (digital magnetic and ancillary) were recovered. The final position data from GPS time and related fiducial time marks (0.1 s intervals) were then merged with digital magnetic and ancillary data traces. Subsequently, a line location file and system log or lead time were produced from the conversion of the merged data (Andreason et al., 2022).

Data Editing: Merged data traces (i.e., the base magnetometer trace) were edited both for completeness and data spikes. The edited and merged data traces were then processed with profile-orientated data corrections (Andreason et al., 2022).

The International Geomagnetic Reference Field (IGRF) Correction: The magnetic data trace was processed with the IGRF correction (Andreason et al., 2022).

Diurnal Correction: The IGRF-corrected magnetic profile data were then processed with the IGRF-corrected diurnal data as a correction (Andreason et al., 2022).

Profile Leveling: An analysis of the network of line crossings was the first stage of leveling undertaken. To ensure that the sum of the square of the mis-tie errors in the network is minimized, the individual survey network lines were systematically shifted down or up. Further constraints were enacted on the systematic corrections to ensure that the sum of the systematic corrections was zero, which can eliminate DC shifts to the network. Virtual Network Analysis (VNA) was used in the micro-leveling process. The VNA is essentially a recursive process where a grid that has been based on the adjusted and edited data forms the starting point. Unadjusted and unedited data were readjusted and reconsidered in the procedure. Ultimately, the recovery of short-wavelength and map-coherent components in the data was made possible with VNA (Andreason et al., 2022).

3.3. Geophysical Data Processing

Here a brief explanation of the raw geophysical data used to create the three different types of maps is presented below, divided by type: topographic, gravity and magnetic (Andreason et al., 2022).

A Shuttle Radar Topography Mission 30 m digital topography data set was utilized to define potential shallow fracture zones in the survey area (NASA JPL, 2013).

Gravity maps, from Earthfield's proprietary North American Gravity Compilation, were used to define density boundaries to illustrate sedimentary structures and fault zones at the basement surface. Bouguer gravity maps processed with a 50, 25, and 25 thousand-feet (kft) wavelength high pass filters were used in enhancing subtle anomalies from shallower sources by removing long wavelength anomalies from sources at depth. A tilt derivation of the gravity data was compiled to enhance lithologic changes and/or fault zones (lateral boundary anomalies) (Andreason et al., 2022). Tilt derivation and high pass filtered maps were used to define basement faults and trends using Werner deconvolution (Werner, 1953).

High-resolution magnetic survey data were used to construct a total magnetic intensity map. Also, a Reduction-to-the-Pole (RTP) map was constructed from the total magnetic intensity map, which shifts magnetic anomalies directly over causative bodies by eliminating the Earth's magnetic inclination/declination effects. Various high pass filters were then applied to the RTP data at 25, 10, 6, and 3 kilo-feet (kft) wavelength, which enhance subtle

anomalies from shallower sources by removing long wavelength anomalies from sources at depth. Additionally, using similar techniques to enhance magnetic anomalies from subtle sources, an RTP analytic signal map was created from the high-resolution magnetic RTP data to better identify shallower intrusive bodies. A tilt derivation of the magnetic data was compiled to enhance lithologic changes and/or fault zones (lateral boundary anomalies) (Andreason et al., 2022). The tilt derivation and high pass filtered maps were useful to define basement faults and trends using Werner deconvolution (Andreason et al., 2022).

3.4. Geophysical Mapping Methods

The creation of the depth-to-basement with basement lineaments, igneous bodies, and the structural high maps by Earthfield Technology LLC is described in Text S1 in Supporting Information S1 (Andreason et al., 2022). Additional processing information related to Werner Deconvolution depth-to-source generation is in Text S1 in Supporting Information S1. In addition to the newly acquired high-resolution magnetic data, gravity data, topography data, and magnetic and gravity depth profiles were incorporated into the depth-to-basement mapping.

Basement lineaments were generated during the depth-to-basement mapping using Werner Deconvolution analysis of the gravity and magnetic data (Andreason et al., 2022). Basement faults were mapped in areas where gradients in the gravity and magnetic data have been identified. Tilt derivative Bouguer gravity data and high-pass filtered (50 and 25 kft) Bouguer gravity data along with tilt derivative RTP magnetic data, and high-pass filtered (25, 10, 6, and 3 kft) RTP magnetic data were used to qualitatively aid in the definition of basement faults and trends originally calculated using Werner deconvolution (Andreason et al., 2022).

The interpreted intrusive bodies and dikes map was produced from various filters and derivative maps of the magnetic data, and by using Werner Deconvolution depth estimation profiles (Andreason et al., 2022). Shallow intrusive bodies were identified using an RTP analytic signal map, which enhances shallow magnetic anomalies at the expense of longer wavelength magnetic anomalies (deeper sources). The new smaller grid spacing allowed delineation of more discrete igneous bodies compared to regional magnetic data (Andreason et al., 2022).

First, using Werner Deconvolution depth analysis, a depth-to-basement map was created (Andreason et al., 2022). This map was subsequently used to create a residual basement map. More specifically, the residual flattened basement map was created via frequency filtering to remove regional dip for the purpose of isolating the local basement high features, and enhancing subtle basement structures. Subsequently, we windowed local high areas at the steepest gradients in the flattened surface to keep only the local highs. Since this residual basement was created using a high pass filter of the original depth-to-basement surface, the units are arbitrary (Andreason et al., 2022).

3.5. Probability Density Mapping

Statistical tests were used to determine whether the spatial relationship between basement faults and intrusions, to observed economic He gas ($>0.3\%$) ($n = 138$) (Brennan et al., 2021; Halford et al., 2022), is significant. Several of the 138 economic He producing wells have multiple He measured values at the same well location. To mitigate data duplication causing confirmation bias, we condensed the original 138 entries into 94 by averaging He values at the same location and within the same formation/substage. To determine whether the distribution of economic He wells ($n = 94$) and structural features (basement faults/intrusions) are spatially correlated, five synthetic grids of randomly generated points ($n = 94$) were created in the study area. Distances to structural features were calculated for each of the synthetic and observed (He-rich gas) data grids. One-way analysis of variance (ANOVA) tests were conducted on the observed and synthetic data grid distances to He occurrences (McKillup & Dyar, 2010) (further discussed in Section 3.6 and Text S2 in Supporting Information S1).

Probability density figures, which represent the relative probability of He occurrences in relation to a structural feature, were created based on the horizontal distance from observed economic He wells to basement lineaments/faults, and intrusions. To create the figures, the distance from all wells containing economic He to the nearest structure was determined. Igneous body locations were calculated from an intermediate depth to produce a simple polygon footprint, when in reality an igneous body can be complex (i.e., interleaved contact zone). Similarly, faults are seldom single linear features and often complex fracture zone systems. To represent these complexities, half-normal distributions were chosen to resemble geological conditions. When examining the possibility that the relationship between the observed economic data and the synthetic data has arisen from chance or not, we

observed that the synthetic data broadly fits a half normal distribution. Thus, in order to compare the synthetic data with the observed economic data, we also utilized a half normal distribution approach when constructing our probability density models with the observed economic data. Thus, a normalized histogram of the distances with a half-normal distribution fit for faults and intrusions was then constructed.

A blank grid of 20,000 equally spaced points (i.e., a finer grid than the original flight and tie line spacing) was created for the study area. The distance from each of the grid points to the different structural features (e.g., fault or intrusion) was determined. Using a Gaussian equation fit to the half normal curve generated for the observed data, the distance to the structural features was input as the X variable value, and the Y variable was calculated (relative probability), which is a value from 0 to 1. Points were then assigned a 0–1 probability value and contour maps with an inverse distance weighted (IDW) interpolation were created.

3.6. Statistical Tests

Pearson's and Kendall's correlations were used to determine the first order relationship concerning the distances between ($n = 94$) economic He wells (>0.3 He %) and basement faults and igneous intrusions (Kendall, 1938; McKillup & Dyar, 2010). The Pearson correlation coefficient (r) examines the extent that two variables are linearly related (McKillup & Dyar, 2010). General assumptions of Pearson's correlation are that the data is generally normally distributed, a linear relationship is present, variables should be continuous, and there should be no significant outliers (McKillup & Dyar, 2010). Kendall's (τ) correlation is a non-parametric measure of the correlation between ranked data that operates under the assumptions of a monotonic relationship and continuous scale or ordinal scale data (Kendall, 1938). The coefficients and their respective p -values comparing economic He and basement faults are: $r = -0.41$ | $p < 0.001$; and $\tau = -0.19$ | $p < 0.006$. The coefficients and their respective p -values comparing economic He and igneous bodies are: $r = -0.53$ | $p < 0.001$; and $\tau = -0.34$ | $p < 0.001$.

The generalized linear model (GLM), which is a type of general class of linear model for independent data, is made up of three components: random, systematic, and a link function (McCullagh & Nelder, 1989). Regarding the residuals, the GLM allows distributions from the exponential family to be permissible (McCullagh & Nelder, 1989). Regarding the relationship between the response and explanatory variables, a linear relationship is required via the link function (McCullagh & Nelder, 1989). Utilizing a Gaussian family distribution and an identity link function, a GLM with the dependent variable as He % and covariates as distance to faults and distance to intrusions showed that basement faults ($p < 0.001$) and igneous bodies ($p < 0.001$) were statistically significant predictor variables concerning He % (Table S1 in Supporting Information S1).

A one-way ANOVA test for significant differences between multiple independent groups. Although the ANOVA test relies on assumptions of independence, normality, and similar variance, it is nonetheless robust with respect to violations of its normality and variance assumptions, especially with larger sample sizes and equal sample sizes (Blanca et al., 2017; Glass et al., 1972; Harwell et al., 1992). The initial hypothesis of the test states that the means are always equal according to the null hypothesis and that at least one mean is different according to the alternative hypothesis. Essentially, the ANOVA test examines between group and within group variation to calculate the F statistic. The calculated F statistic is compared to a critical F statistic. When the calculated F statistic is greater than the critical value (critical F statistic), the null hypothesis is rejected (the sample populations are different, i.e., they do not have the same mean), and the alternative hypotheses are adopted (McKillup & Dyar, 2010).

The synthetic data set represents randomly distributed pseudo-wells, while the observed data points are observed economic He wells. To keep sample sizes similar to the economic data ($n = 94$), 94 locations were randomly selected from each of the synthetic grids. The ANOVA single factor statistical tests were conducted to check for any significant variations when comparing the synthetic grids ($n = 94$) and no significant differences were found (Tables S2 and S5 in Supporting Information S1). Additionally, ANOVA tests were conducted with the five synthetic grids and the economic data sets. This second ANOVA test showed that there was a significant difference present in the economic and synthetic data sets for both faults and intrusions (F statistic $> F$ critical value; $p < 0.001$). A Games-Howell post hoc test, which is a non-parametric approach that does not rely on homogeneity of variances, was used to examine combinations of group differences (McKillup & Dyar, 2010; Ruxton & Beauchamp, 2008). Comparing the economic data to the synthetic data for both faults and intrusions produced a Games-Howell post hoc test p value of <0.001 , which can be interpreted as the economic He data being significantly different from the synthetic data and thus the economic He data are not randomly distributed (Tables S3, S4, S6, and S7 in Supporting Information S1). Despite heteroscedasticity (non-homogenous variances) in our

data sets reducing the statistical power of the one way ANOVA test, the ANOVA tests still produced a significant effect, showing that any heterogeneity of variance does not skew the results.

4. Results

4.1. Spatial Correlations Between Structural Features and High-He Occurrences

Statistically significant relationships between high-He fields and structural features (basement faults, igneous intrusions, and basement structural highs) are observed in coupled high-resolution geophysical and geochemical data sets (Figure 1). These correlations were not observed utilizing proprietary interpretations of low-resolution geophysical data due to the significantly larger line spacing (i.e., 4.8 km by 14.5 km spacing lines) in relation to the structures of interest (EG & G GeoMetrics, Inc, 1979; U.S. Geological Survey, 1980).

Within the Four Corners area, all economic He observations occur within 0 to ~2.5 and ~4.5 km of faults and intrusions, respectively. In contrast, synthetically generated data points occur within 0–6 km of these features (Figures 2 and 3). Figures 2 and 3 were constructed to test the assumption that the geospatial distributions of basement faults and intrusions are the dominant contributors to economic (<0.3 He %) He plays. Histograms (Figures 2b and 3b) illustrate the striking inverse relationship between wells with observed economic He gas values and the lateral distance to basement faults and intrusions. As He molar % increases, the distance to the structural feature decreases, indicating that higher He concentration is correlated with shorter distances to basement faults and intrusions, consistent with the hypothesis that they provide a linkage from source rocks at depth to a shallower reservoir, which has an adequate trapping/sealing mechanism.

Examining distances to structural features, the data of the economic He wells shows that 88% are <1 km from basement faults, and 85% of economic He wells (>0.3 He %) are <1 km from intrusions (Figures 2b and 3b). The observed economic He wells are left skewed with most data points restricted to <1 km from both faults and intrusions, while the synthetic data are evenly distributed (Figures 2c and 3c). ANOVA *F* statistics (*F*-faults 7.11, *p* < 0.001; *F*-intrusions 17.48, *p* < 0.001) > *F* critical values (2.23 for both) and post hoc tests (Text S2 in Supporting Information S1) show the spatial relationships between economic He and faults and intrusions are not controlled by random processes (Tables S2–S7 in Supporting Information S1). Thus, by comparing observed and synthetic data sets, we find that their relative density distributions are statistically different, suggesting that a non-random process is controlling their relationship.

We found no observed correlation between high-He occurrence and other structural features, including basement depth, dike cluster locations, reservoir depth compared to basement depth, position on structural basement structure, distance to basement structural highs, and sealing intervals. Additionally, it was not possible to test any intrusion depth correlation with He occurrence due to low data density. A topological analysis was completed to examine the relationship between He occurrence and fault connectivity/geometry; however, we found that He is not strongly correlated with basement fault connectivity compared to the relationship with He and basement faults shown in Figure 1, and as such we do not pursue further 2-D connectivity mapping (Text S3 in Supporting Information S1).

To summarize, using a spatial and statistical analysis of He occurrence with faults and intrusions from high-resolution geophysics, our results demonstrate that a non-random process indeed controls the relationship between He and faults and intrusions. Additionally, there is a strong relationship between He and faults/intrusions that can be quantified and utilized for He exploration as a primary target.

5. Discussion

5.1. He-System Processes Related to Faults and Intrusions

Migration of He from its source to the surface is likely enhanced by a thermal perturbation (i.e., geothermal setting) of the crust (Cheng et al., 2021, 2023; Danabalan et al., 2022; Lowenstern et al., 2014; Torgersen, 2010). This has an effect on multiple scales. An increase in thermal gradient will enhance He release from minerals by exceeding the closure temperature, and promote the release of related gases such as nitrogen (N₂) by low-grade metamorphism (e.g., Ballentine & Lollar, 2002). While heat flow in facilitating helium release from basement rocks plays a role in the regional mobilization of He into the overlying sedimentary column, we observe no

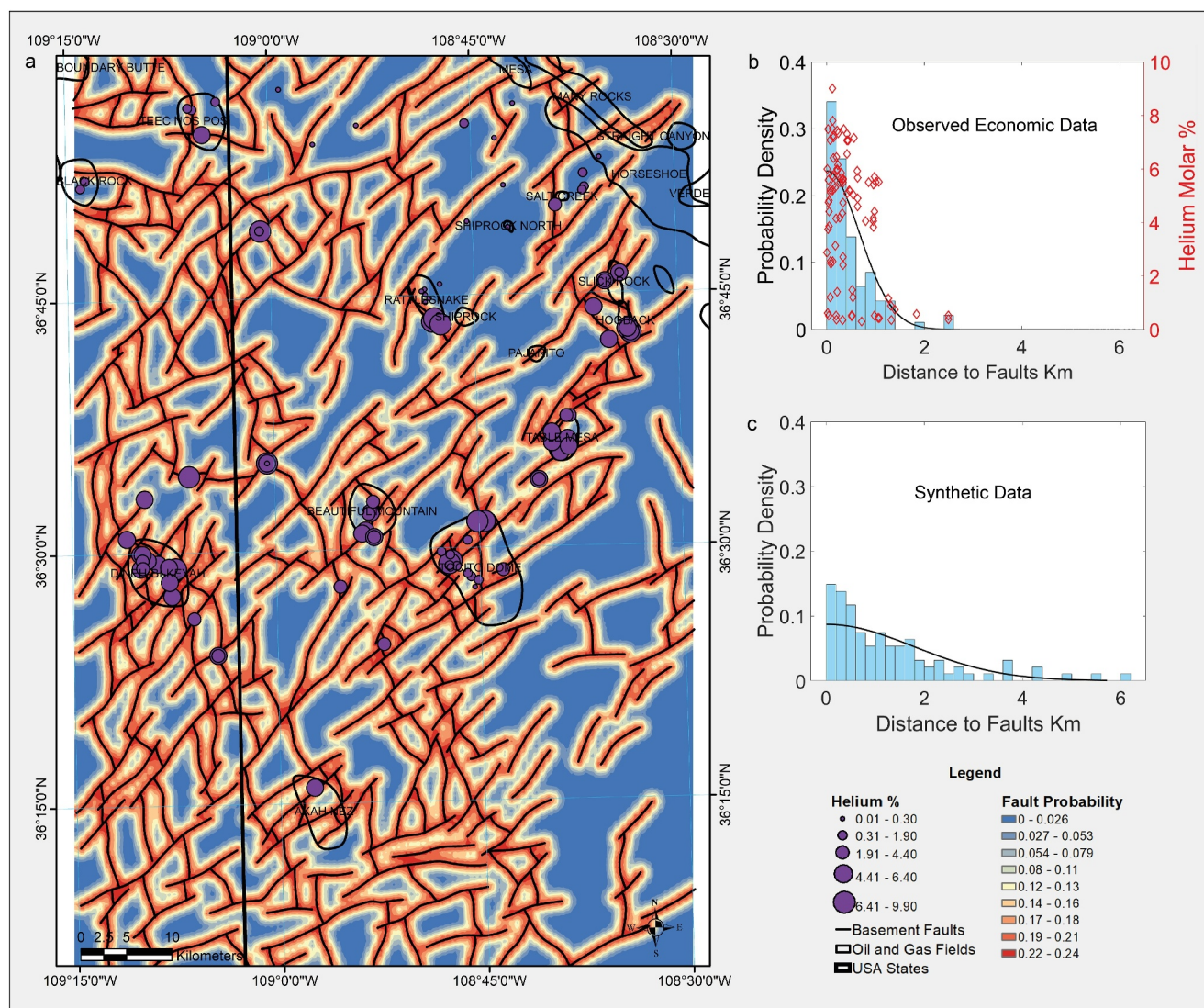


Figure 2. (a) Probability density figure for He occurrence with basement faults (b) Histogram with a half normal distribution (black curve) showing distances from basement faults to economic He wells ($n = 94$). Economic He data ($n = 94$) is overlain (red diamonds) (Brennan et al., 2021; Halford et al., 2022). (c) Synthetic grid data, which is shown with a half normal distribution (black curve), has a statistically different distribution (F value 7.11 > F critical value 2.23 in Text S2 in Supporting Information S1) when compared to the economic data (b) shows a non-random process controlling the relationship between He and basement faults (mod. from Andreason et al., 2022).

significant trends between calculated modern heat flow and He % in the localized area of interest (Text S4 in Supporting Information S1).

Regarding subsurface faulting, interconnected fractures and pore space, perhaps enhanced by the He- and N_2 -rich fluid pressure exceeding the lithostatic confining pressure, promote advective movement of He from the source rock (Danabalan et al., 2022; Warr et al., 2018). Zones of enhanced porosity and permeability such as faults reasonably act to focus the fluids released. Basement faults act as migration conduits, allowing the He- and nitrogen-rich fluids to migrate updip to a structural or stratigraphic trap driven by gas buoyancy or pressure differentials (Danabalan et al., 2022; Halford et al., 2022). Whether the deep-seated basement faults propagate all the way to the reservoir is unknown, but due to their interpreted dimensions at depth, their presence remains critical. Thus, basement faults are interpreted to be the controlling agent aiding in primary migration (i.e., He advective transport) from the source rock into the overlying sedimentary column as well as in secondary migration (Danabalan et al., 2022; Halford et al., 2022).

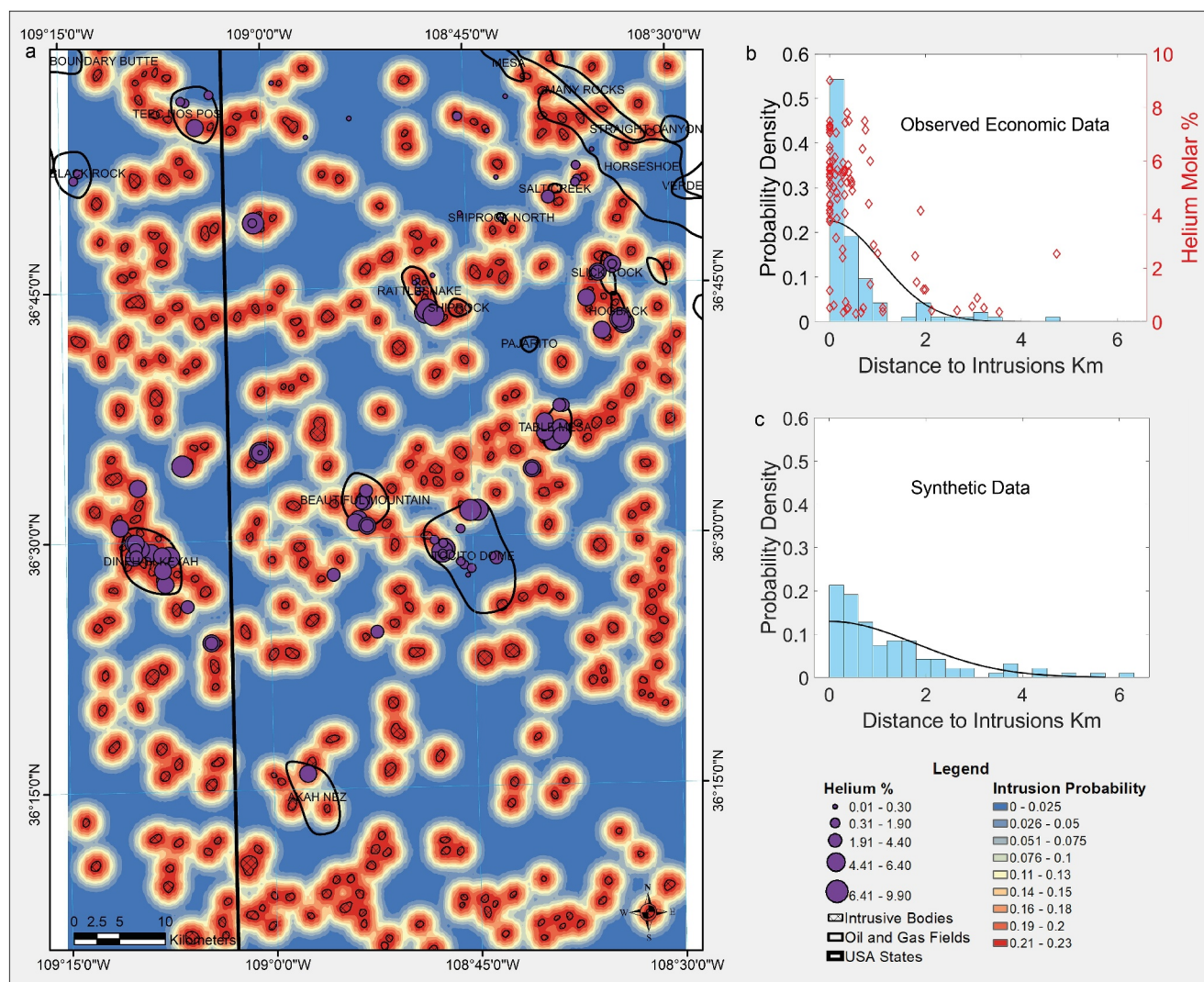


Figure 3. (a) Probability density figure for He occurrence with intrusions (b) Histogram with a half normal distribution (black curve) showing distances from intrusions to economic He wells ($n = 94$). Economic He data ($n = 94$) is overlain (red diamonds) (Brennan et al., 2021; Halford et al., 2022) (c) Synthetic grid data, which is shown with a half normal distribution (black curve), has a statistically different distribution (F value 17.48 > F critical value 2.23 in Text S2 in Supporting Information S1) when compared with the economic data (b) shows a non-random process controlling the relationship between He and intrusions (mod. from Andreason et al., 2022).

In principle, intrusions may provide local heating and some He release from minerals. Intrusions will also enhance any fracture network by increasing hydrothermal fluid and magma pressures, likely following pre-existing zones of weaknesses as well as providing supplemental shallow radial and concentric fracturing (Gonzales & Lake, 2017; Halford, 2018; Koide & Bhattacharji, 1975; Re et al., 2015). Like faults, intrusions also provide a focus for He- and N_2 -rich fluid collection at depth in the crust and a transport pathway to the near surface (Ballentine et al., 2002; Broadhead & Gillard, 2004; Halford, 2018). Additionally, given that intrusions likely transport other volatiles (such as CO_2), the potential for dilution or lack thereof of He from volatiles associated with the intrusions should be considered. Similarly, whether the intrusion invades the reservoir or breaches the basement is yet to be determined based on the inherent challenges (i.e., processing costs, different igneous body geometries, different mineral compositions, etc.) of calculating exact intrusion depth. Since most He occurrences lie <1 km of an intrusion, we interpret this as evidence to support a strong component of primary and secondary vertical migration (depending on how far the intrusion invades) coupled with a weak component of lateral secondary migration (Halford et al., 2022).

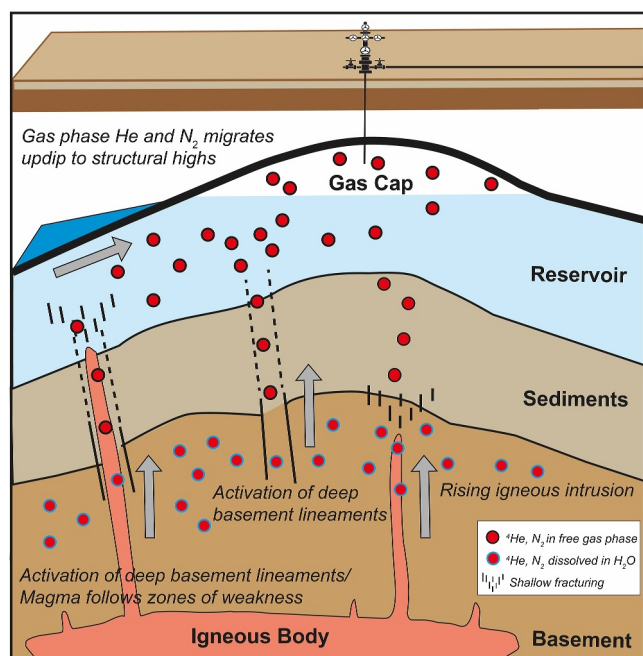


Figure 4. Schematic illustrating the conceptual model showing the activation of deep basement lineaments/faults, and continued igneous activity, which equates to an increased supplemental shallow fracturing followed by He migration upwards along the zones of weakness, and He migration updip to structural highs. Regarding shallow fracturing, when hydrothermal fluid and magma pressures are lower (but higher than lithostatic stress), there is the formation of predominant radial fractures. Additionally, when there is an increase in hydrothermal fluid and magma pressures, we predict an increase in peripheral radial fractures and concentric fracture patterns (not shown) surrounding intrusions (mod. from Halford et al., 2022; Koide & Bhattacharji, 1975; Van Zalinge et al., 2022).

In summary, to update the role of faults and intrusions in relation to helium's migration and trapping, a schematic is presented that describes how basement faults and igneous intrusions or a combination of both can act as migration/focusing conduits (Figure 4). Intrusions can also provide local heating to release He from minerals as well as provide supplemental fracturing, which likely enhances fluid flow. Thus, the strong spatial statistical correlation of He wells to both basement faults and intrusions suggests that advective transport via faults/intrusions facilitates He flow/transport (primary and secondary migration) of basement derived He into the overlying sediments where the He can accumulate over time in a structural or stratigraphic trap (Figure 4).

5.2. Combined Predictive Probability Mapping for Helium Occurrence

The close proximity of economic He wells and structural features is reflected in the relative probability density figures, which show areas of higher probabilities (colored as red intervals) of encountering economic subsurface He based on basement fault and intrusion data (Figures 2 and 3). Figures 2 and 3 show that both faults and intrusions correlate with high-He, and to a similar magnitude. We created a composite figure to consider the combined relative probabilities of both faults and intrusions (Figure 5). Because there is no a priori reason to differentially weight these features, we use the multiplication rule with faults and intrusions equally weighted as independent variables. The composite figure, with an IDW interpolation and normalized to 1, illustrates low (blue) to high (red) areas of inferred probability of high-He occurrences (Figure 5).

Of all the identified economic He wells, 88% lie within the basement structural high zones (Figure 1d), with 91% of the remaining He points plotting near (<1 km) igneous bodies, which are likely creating subsurface domes as the igneous body moves through the subsurface enhancing structural trapping. Regarding basement structural highs, we make the simplifying assumption that basement highs should correlate to domal deformation of the overlying sedimentary cover that could produce ideal

conditions to form an economic structural trap for He. Local structural maps, which highlight the strong relationship of He to relative structural highs, are presented in Text S4 in Supporting Information S1 for the Herich Dineh-Bi-Keyah, Tocito Dome and Teec Nos Pos fields (Figures S2–S6 in Supporting Information S1). While structural highs are an essential component of the trapping mechanism, we do not consider them a feature that enhances He migration via transport from the crystalline basement. Therefore, to visualize where the He (focused via faults and intrusions) could be trapped, we overlay the structural basement high boundaries (Section 3.4) onto the composite figure (Figure 5) rather than including these structural highs within the combined He occurrence probability.

The highest likelihood of an economic He accumulation is where the combined probability of the influence of basement faults and intrusions is closest to 1 (the intersections of the red colored intervals), providing proximity to both the pathways that would appear to promote He transport to the near surface. The presented combined probability figure (Figure 5) treats faults and intrusions as independent events; however, there is a natural propensity of both to exploit zones of crustal weakness. Both faults and intrusions play a part in He release, mobilization, and transport, and some of the effects may overlap—and are provided an equal weighting.

To summarize, by constructing a probabilistic relationship as a function of distance from basement faults and intrusions, we have developed a predictive model for high-He gas field occurrence. The probability analysis highlights the importance of targeting zones at the intersection of basement faults and intrusions, as well as provides confirmation of the role of gas phase buoyancy and structural trapping. With regard to He exploration, the predictive exploration model can be translated to other areas to generate He prospects, especially near regional/local thermal perturbations and active tectonics.

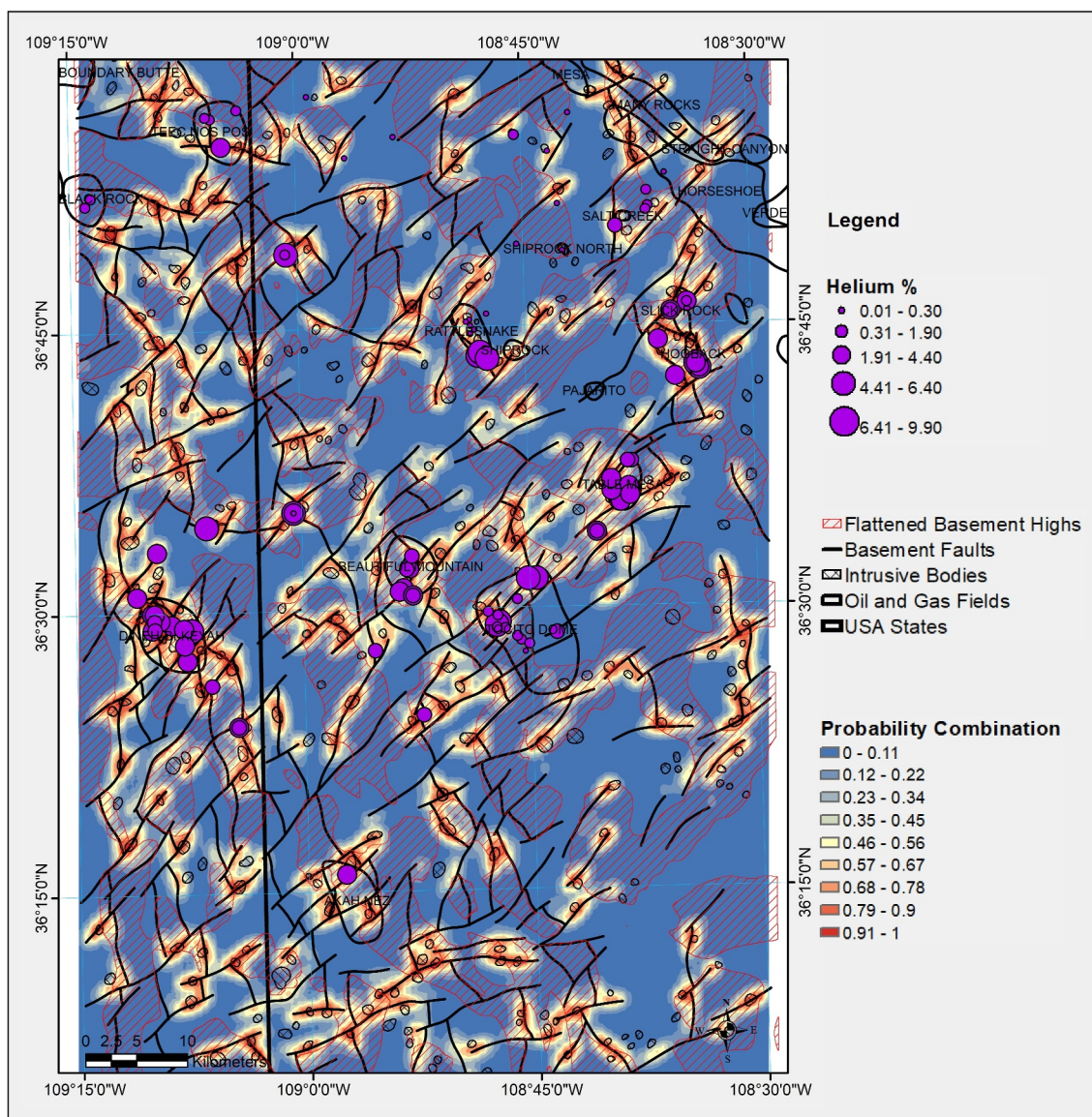


Figure 5. Composite probability figure combining the basement fault and the intrusion He occurrence probabilities along with an outline of localized basement structural highs. The predictive exploration model shows that the intersection of faults/intrusions (He transport mechanism) and basement highs (He trapping mechanism) are the zones of interest (mod. from Andreason et al., 2022; Brennan et al., 2021; Halford et al., 2022).

6. Conclusion

The importance of dominant structural mechanisms such as basement faults and intrusions in the transport of He from a deep crustal source to reservoir has been speculated before (Danabalan et al., 2022; Halford et al., 2022; Karolyte et al., 2022), together with circumstantial evidence of basement fault control (Boles et al., 2015; Buttitta et al., 2020; Craddock et al., 2017; Mtili et al., 2021; Tardani et al., 2016). Using a spatial analysis of He occurrence with faults and intrusions from high-resolution geophysics, we show that a non-random process indeed controls the relationship between He and faults and intrusions and that there is a strong relationship between He and faults/intrusions that can be quantified and utilized.

By constructing a probabilistic relationship as a function of distance from these features, we have developed a predictive model. The probability analysis highlights the importance of targeting zones at the intersection of basement faults and intrusions. The significance of this study is threefold. It (a) provides a quantitative spatial analysis of basement faults and intrusions for He exploration, (b) presents a predictive exploration model that can

be translated to other areas to generate He prospects, especially near regional/local thermal perturbations and active tectonics, and (c) updates geologic elements and processes of the He-system (migration and structural trapping of He).

Data Availability Statement

Helium geochemical data supporting this research are included in Brennan et al. (2021), <https://doi.org/10.5066/P92QL79J>, Halford (2018, 2023), and Halford et al. (2022), <https://doi.org/10.1016/j.chemgeo.2022.120790>. Maps of the high-resolution geophysical data supporting this research can be found in Andreason et al. (2022). Raw high-resolution geophysical data supporting this research are not accessible to the public or the research community. Inquiries should be directed to the Navajo Nation Division of Natural Resources, Navajo Minerals Department (<https://dnr.navajo-nsn.gov/Departments>), and the Navajo Nation Oil and Gas Company (<https://nnogc.com/contact-us/>).

Spatial processing software (ArcGIS suite) supporting this research is available through ESRI. General plotting software (Excel, Illustrator, MATLAB) supporting this research is available through Microsoft, Adobe, and MathWorks, respectively. The statistical software package (JASP) supporting this research is available at no cost from <https://jasp-stats.org/> (JASP Team, 2023). Geophysical processing software supporting this research is not accessible to the public or the research community. Inquiries should be directed to Earthfield Technologies, LLC.

Acknowledgments

This research was supported by the University of Oxford Noble Laboratory, the University College Oxford-Radcliffe Scholarship, the Navajo Nation Oil and Gas Company (NNOGC), and the Division of Energy and Mineral Development (Bureau of Indian Affairs). We are thankful to the Navajo Nation and Navajo Minerals Department for their support. We are grateful for the independent release of preliminary Navajo Nation data and interpretation made public by the Navajo Nation Oil and Gas Company on April 2024 into the public domain from an internal study (unrefereed preprint) funded with an Energy and Mineral Development Program grant through the U.S. Bureau of Indian Affairs. Discussions with Benjamin Bymers, Nadia Chernyak, Paul Differding, Darren Hillemonds, Ryan Lambrecht, and Cassidy Wolfe benefited this work. We kindly thank Dr. Hunt and an anonymous reviewer for their comments that enhanced the quality of the paper. The project was conceived by DTH, RK, MWA, JJC, KJWM, JGG, and CJB. DTH managed the project, and prepared the first draft of the manuscript. BC and MC collected and processed the geophysical data. Geophysical data visualizations were produced and made available by BC, MC, JJC, and JTD. Structural maps were constructed by DTH, JJC, and SS. Probabilistic geospatial and statistical models were developed by DTH, RK, AC, and CJB. All authors contributed to the final manuscript.

References

- Anderson, S. T. (2018). Economics, helium, and the U.S. Federal helium reserve: Summary and outlook. *Natural Resources Research*, 27(4), 455–477. <https://doi.org/10.1007/s11053-017-9359-y>
- Andreason, M. W., Cathey, B., Cathey, M., & Rice, G. K. (2022). *Identification and maturation of new potential helium deposits on the Navajo Nation lands, internal grant deliverable completed by the Navajo Nation oil and gas Co., Earthfield Technology LLC and GeoFrontiers Corp.* Funded through the Division of Energy and Minerals Development - Energy and Mineral Development Program Grant #A21AP10056 awarded to the Navajo Nation. Retrieved from https://nnogc.com/wp-content/uploads/2024/04/FINAL-REPORT-HELIUM-NAVAJO-NATION_APR2022.pdf
- Ballentine, C. J., Burgess, R., & Marty, B. (2002). Tracing fluid origin, transport and interaction in the crust. *Reviews in Mineralogy and Geochemistry*, 47(1), 539–614. <https://doi.org/10.2138/rmg.2002.47.13>
- Ballentine, C. J., & Lollar, B. S. (2002). Regional groundwater focusing of nitrogen and noble gases into the Hugoton-Panhandle giant gas field, USA. *Geochimica et Cosmochimica Acta*, 66(14), 2483–2497. [https://doi.org/10.1016/S0016-7037\(02\)00850-5](https://doi.org/10.1016/S0016-7037(02)00850-5)
- Béllanger, C., & Ross, P. S. (2018). Origin of nonbedded pyroclastic rocks in the Cathedral Cliff diatreme, Navajo volcanic field, New Mexico. *Bulletin of Volcanology*, 80(61), 61. <https://doi.org/10.1007/s00445-018-1234-0>
- Blanca, M. J., Alarcón, R., Arnau, J., Bono, R., & Bendayan, R. (2017). Non-normal data: Is ANOVA still a valid option? *Psicothema*, 29(4), 552–557. <https://doi.org/10.7334/psicothema2016.383>
- Boles, J. R., Garven, G., Camacho, H., & Lupton, J. E. (2015). Mantle helium along the newport-Inglewood fault zone, Los Angeles basin, California: A leaking paleo-subduction zone. *Geochemistry, Geophysics, Geosystems*, 16(7), 2364–2381. <https://doi.org/10.1002/2015GC005951>
- Boreham, C. J., Edwards, D. S., Poreda, R. J., Darrah, T. H., Zhu, R., Grosjean, E., et al. (2018). Helium in the Australian liquefied natural gas economy. *Journal of the Australian Petroleum Production and Exploration Association (APPEA)*, 58(1), 209–237. <https://doi.org/10.1071/AJ17049>
- Brennan, S., East, J., Dennen, K., Jahediesfanjani, H., & Varela, B. (2021). Helium concentrations in United States wells. In *U.S. Geological Survey Scientific Investigations Report 2021–5085* (Vol. 5). <https://doi.org/10.5066/P92QL79J>
- Broadhead, R. F., & Gillard, L. (2004). Helium in New Mexico: Geologic distribution and exploration Possibilities. In *Open file report no. 483*. New Mexico Bureau of Geology and Mineral Resources, A Division of New Mexico Tech, Socorro, NM. <https://doi.org/10.58799/OFR-483>
- Buttitta, D., Caracausi, A., Chiaraluce, L., Favara, R., Gasparo Morticelli, M., & Sulli, A. (2020). Continental degassing of helium in an active tectonic setting (northern Italy): The role of seismicity. *Scientific Reports*, 10(1), 162. <https://doi.org/10.1038/s41598-019-55678-7>
- Casey, T. A. L. (1983). Helium potential of the Four Corners area. In J. E. Fassett (Ed.), *Oil and gas fields of the Four Corners area* (Vol. III, pp. 749–754). Four Corners Geological Society.
- Cheng, A., Sherwood Lollar, B., Gluyas, J. G., & Ballentine, C. J. (2023). Primary N₂-He gas field formation in intracratonic sedimentary basins. *Nature*, 615(7950), 94–99. <https://doi.org/10.1038/s41586-022-05659-0>
- Cheng, A., Sherwood Lollar, B., Warr, O., Ferguson, G., Idiz, E., Mundle, S. O. C., et al. (2021). Determining the role of diffusion and basement flux in controlling ⁴He distribution in sedimentary basin fluids. *Earth and Planetary Science Letters*, 574, 117175. <https://doi.org/10.1016/j.epsl.2021.117175>
- Craddock, W. H., Blondes, M. S., DeVera, C. A., & Hunt, A. G. (2017). Mantle and crustal gases of the Colorado Plateau: Geochemistry, sources, and migration pathways. *Geochimica et Cosmochimica Acta*, 213, 346–374. <https://doi.org/10.1016/j.gca.2017.05.017>
- Danabalan, D., Gluyas, J. G., Macpherson, C. G., Abraham-James, T. H., Bluett, J. J., Barry, P. H., & Ballentine, C. J. (2022). The principles of helium exploration. *Petroleum Geoscience*, 28(2), 2021–2029. <https://doi.org/10.1144/petgeo2021-029>
- Danie, T. C. (1978). Dineh-bi-Keyah (oil), 1978, T. 35-36 N., R. 29-30 E., G&SRM Apache County, Arizona. In *Four Corners geological society, oil and gas fields of the Four Corners area* (Vol. I–II, pp. 73–76).
- Davis, G. H., & Bump, A. P. (2009). Structural geologic evolution of the Colorado Plateau. In S. M. Kay, V. A. Ramos, & W. R. Dickinson (Eds.), *Backbone of the Americas: Shallow subduction, plateau uplift, and ridge and Terrane Collision: Geological Society of America memoir* (Vol. 204, pp. 99–124). [https://doi.org/10.1130/2009.1204\(05\)](https://doi.org/10.1130/2009.1204(05))

- Delaney, P. T. (1987). Ship rock, New Mexico: The vent of a violent volcanic eruption. In S. S. Beus (Ed.), *Geological society of America centennial field guide, Rocky Mountain section, Boulder* (Vol. 2, pp. 411–415). <https://doi.org/10.1130/0-8137-5402-x.411>
- EG & G GeoMetrics, Inc. (1979). National uranium resource evaluation aerial gamma ray and magnetic survey, Raton basin project, Shiprock and Gallup quadrangles, Arizona/New Mexico and Albuquerque quadrangle, New Mexico-final report: U.S. Department of Energy Grand Junction Office [Report] GJBX 116-79, volume 2, n.p., scale 1:500,000.
- Gilfillan, S. M. V., Ballentine, C. J., Holland, G., Sherwood Lollar, B., Stevens, S., Schoell, M., & Cassidy, M. (2008). Natural CO₂ storage analogues: The noble gas geochemistry of natural CO₂ gas reservoirs from the Colorado Plateau and Rocky Mountain provinces, USA. *Geochimica et Cosmochimica Acta*, 72(4), 1174–1198. <https://doi.org/10.1016/j.gca.2007.10.009>
- Glass, G. V., Peckham, P. D., & Sanders, J. R. (1972). Consequences of failure to meet assumptions underlying fixed effects analyses of variance and covariance. *Review of Educational Research*, 42(3), 237–288. <https://doi.org/10.3102/00346543042003237>
- Gonzales, D. A., & Lake, E. T. (2017). Geochemical constraints on mantle-melt sources for Oligocene to Pleistocene mafic rocks in the Four Corners region, USA. *Geosphere*, 13(1), 201–226. <https://doi.org/10.1130/GES01314.1>
- Halford, D. T. (2018). *Isotopic analyses of helium from wells located in the Four Corners area, Southwestern, USA. [Master's thesis]*. Colorado School of Mines. Mines Repository. Retrieved from <https://repository.mines.edu/handle/11124/172822>
- Halford, D. T. (2023). *Geologic processes that control sourcing and migration of subsurface helium [PhD thesis]*. University of Oxford. <https://doi.org/10.5287/ora-00zdnvm4m>
- Halford, D. T., Karolytė, R., Barry, P. H., Whyte, C. J., Darrah, T. H., Cuzella, J. J., et al. (2022). High helium reservoirs in the Four Corners area of the Colorado plateau, USA. *Chemical Geology*, 596, 120790. <https://doi.org/10.1016/j.chemgeo.2022.120790>
- Harwell, M. R., Rubinstein, E. N., Hayes, W. S., & Olds, C. C. (1992). Summarizing Monte Carlo results in methodological research: The one- and two-factor fixed effects ANOVA cases. *Journal of Educational Statistics*, 17(4), 315–339. <https://doi.org/10.2307/1165127>
- Hernández-Urbe, D., & Palin, R. M. (2019). Catastrophic shear-removal of subcontinental lithospheric mantle beneath the Colorado Plateau by the subducted Farallon slab. *Scientific Reports*, 9(1), 8153. <https://doi.org/10.1038/s41598-019-44628-y>
- JASP Team. (2023). JASP (Computer software). Retrieved from <https://jasp-stats.org/>
- Karlstrom, K. E., & Humphreys, E. D. (1998). Persistent influence of Proterozoic accretionary boundaries in the tectonic evolution of southwestern North America: Interaction of cratonic grain and mantle modification events. *Rocky Mountain Geology*, 33(2), 161–179. <https://doi.org/10.2113/33.2.161>
- Karolytė, R., Warr, O., Van Heerden, E., Flude, S., De Lange, F., Webb, S., et al. (2022). The role of porosity in H₂/He production ratios in fracture fluids from the Witwatersrand Basin, South Africa. *Chemical Geology*, 595, 120788. <https://doi.org/10.1016/j.chemgeo.2022.120788>
- Kendall, M. G. (1938). A new measure of rank correlation. *Biometrika*, 30(1–2), 81–89. <https://doi.org/10.1093/biomet/30.1-2.81>
- Koide, H., & Bhattacharji, S. (1975). Formation of fractures around magmatic intrusions and their role in ore localization. *Economic Geology*, 70(4), 781–799. <https://doi.org/10.2113/gsecongeo.70.4.781>
- Lowenstern, J., Evans, W., Bergfeld, D., & Hunt, A. G. (2014). Prodigious degassing of a billion years of accumulated radiogenic helium at Yellowstone. *Nature*, 506(7488), 355–358. <https://doi.org/10.1038/nature12992>
- Masters, J. A. (2000). The slow discovery of Dineh-Bi-Keyah. *Mountain Geologist*, 37(2), 91–100.
- McCullagh, P., & Nelder, J. A. (1989). *Generalized linear models. Monographs on statistics and applied probability*. Chapman and Hall.
- McKillop, S., & Dyar, M. D. (2010). *Geostatistics explained: An introductory guide for Earth scientists*. Cambridge University Press.
- Mili, K. M., Byrne, D. J., Tyne, R. L., Kazimoto, E. O., Kimani, C. N., Kasanzu, C. H., et al. (2021). The origin of high helium concentrations in the gas fields of southwestern Tanzania. *Chemical Geology*, 585, 120542. <https://doi.org/10.1016/j.chemgeo.2021.120542>
- NASA JPL. (2013). NASA Shuttle radar topography mission global 1 arc second [Dataset]. NASA EOSDIS Land Processes DAAC. <https://doi.org/10.5067/MEaSUREs/SRTM/SRTMGL1.003>
- National Research Council. (2010). *Selling the Nation's helium reserve*. The National Academies Press. <https://doi.org/10.17226/12844>
- Olafsdottir, A. H., & Sverdrup, H. U. (2020). Assessing the past and future sustainability of global helium resources, extraction, supply and use, using the integrated assessment model WORLD7. *Biophysical Economics and Sustainability*, 5(6), 6. <https://doi.org/10.1007/s41247-020-00072-5>
- Re, G., White, J. D. L., & Ort, M. H. (2015). Dikes, sills, and stress-regime evolution during emplacement of the Jagged rocks complex, Hopi Buttes volcanic field, Navajo nation, USA. *Journal of Volcanology and Geothermal Research*, 295, 65–79. <https://doi.org/10.1016/j.jvolgeores.2015.01.009>
- Ruxton, G. D., & Beauchamp, G. (2008). Time for some a priori thinking about post hoc testing. *Behavioral Ecology*, 19(3), 690–693. <https://doi.org/10.1093/beheco/arn020>
- Semken, S. (2003). Black rocks protruding up: The Navajo volcanic field. In *New Mexico geological society guidebook, 54th field conference, geology of the Zuni plateau* (pp. 133–138).
- Tardani, D., Reich, M., Rouleau, E., Takahata, N., Sano, Y., Pérez-Flores, P., et al. (2016). Exploring the structural controls on helium, nitrogen and carbon isotope signatures in hydrothermal fluids along an intra-arc fault system. *Geochimica et Cosmochimica Acta*, 184, 193–211. <https://doi.org/10.1016/j.gca.2016.04.031>
- Torgersen, T. (2010). Continental degassing flux of ⁴He and its variability. *Geochemistry, Geophysics, Geosystems*, 11(6), Q06002. <https://doi.org/10.1029/2009GC002930>
- U.S. Geological Survey. (1980). Aeromagnetic map of northeast Arizona and northwest New Mexico: U.S. Geological Survey open-file report 80-614, 4 sheets, scale 1:250,000.
- Van Zalinge, M. E., Mark, D. F., Sparks, R. S. J., Tremblay, M. M., Keller, C. B., Cooper, F. J., & Rust, A. (2022). Timescales for pluton growth, magma-chamber formation and super-eruptions. *Nature*, 608(7921), 87–92. <https://doi.org/10.1038/s41586-022-04921-9>
- Warr, O., Sherwood Lollar, B., Fellowes, J., Sutcliffe, C. N., McDermott, J. M., Holland, G., et al. (2018). Tracing ancient hydrogeological fracture network age and compartmentalization using noble gases. *Geochimica et Cosmochimica Acta*, 222, 340–362. <https://doi.org/10.1016/j.gca.2017.10.022>
- Werner, R. T. (1953). Interpretation of magnetic anomalies at sheet-like bodies. *Sveriges Geologiska Undersok, Series C, Arsbok*, 43(6), 413–449.
- Whitmeyer, S. J., & Karlstrom, K. E. (2007). Tectonic model for the Proterozoic growth of North America. *Geosphere*, 3(4), 200–259. <https://doi.org/10.1130/GES00055.1>

References From the Supporting Information

- Allen, W. E. (1978a). Navajo Springs (helium), T. 19-20 N., R. 27-28 E., G&SRM, Apache County, Arizona. In *Four corners geological Society —Oil and gas fields of the four corners area* (Vol. III, pp. 80–84).

- Allen, W. E. (1978b). Pinta dome (helium), T. 19–20 N., R. 26 E., G&SRM, Apache County, Arizona. In *Four corners geological Society—Oil and gas fields of the four corners area* (Vol. I–II, pp. 85–89).
- Blackwell, D., Richards, M., Frone, Z., Batir, J., Ruzo, A., Dingwall, R., & Williams, M. (2011). Temperature at depth maps for the conterminous US and geothermal resource estimates. *GRC Transactions*, 35, 1545.
- Dunn, P. K., & Smyth, G. K. (2018). *Generalized linear models with examples in R*. Springer. <https://doi.org/10.1007/978-1-4419-0118-7>
- Freeman, W. M. (1978). Aneth (Ratherford Unit) (oil), T. 41 S., R. 23–24 E., SLP, San Juan County, Utah. In *Four corners geological society. Oil and gas fields of the four corners area* (Vol. I–II, pp. 584–586).
- Goss-Sampson, M. A. (2018). Statistical analysis in JASP 0.9.2: A Guide for students. Version 2, October 2018. Retrieved from <https://jasp-stats.org/jasp-materials/>
- Herrmann, R. B., Dewey, J. W., & Park, S. K. (1966). The Dulce, New Mexico, earthquake of 23 January 1966. *Bulletin of the Seismological Society of America*, 70(6), 2171–2183.
- Hoffman, J. P., & Northrup, S. A. (1977). The Dulce, New Mexico earthquake Jan. 23, 1966. *Earthquake Notes*, 48(4), 3–20. <https://doi.org/10.1785/gssrl.48.4.3>
- Jaksha, L. H., & Evans, D. H. (1984). Reconnaissance seismic refraction reflection surveys in Northwestern New Mexico. *Seismological Society of America Bulletin*, 74(4), 1263–1274. <https://doi.org/10.1785/bssa0740041263>
- Jaksha, L. H. (1982). Reconnaissance seismic refraction reflection surveys in southwestern New Mexico. *Bulletin of the Geological Society of America*, 93(10), 1030–1037. [https://doi.org/10.1130/0016-7606\(1982\)93<1030:rsrsis>2.0.co;2](https://doi.org/10.1130/0016-7606(1982)93<1030:rsrsis>2.0.co;2)
- Lastowka, L. A., Sheehan, A. F., & Schneider, J. M. (2001). Seismic evidence for a partial lithospheric delamination model of Colorado Plateau uplift. *Geophysical Research Letters*, 28(7), 1319–1322. <https://doi.org/10.1029/2000gl012360>
- Leidig, M. R., Bonner, J. L., & Reiter, D. L. (2005). Development of a velocity model for Black Mesa, Arizona, and the southern Colorado Plateau from multiple data sets. *Bulletin of the Seismological Society of America*, 95(6), 2136–2151. <https://doi.org/10.1785/0120050004>
- Liu, K., Levander, A., Niu, F., & Miller, M. S. (2011). Imaging crustal and upper mantle structure beneath the Colorado Plateau using finite-frequency Rayleigh wave tomography. *Geochemistry, Geophysics, Geosystems*, 12(7), Q07001. <https://doi.org/10.1029/2011gc003611>
- Lutter, W. J., Roberts, P. M., Thurber, C. H., Steck, L., Fehler, M. C., Stafford, D. G., et al. (1995). Teleseismic P-wave image of crust and upper mantle structure beneath the Valles caldera, New Mexico: Initial results from the 1993 JTEX passive array. *Geophysical Research Letters*, 22(4), 505–508. <https://doi.org/10.1029/94gl03220>
- McCowan, D. W. (1978). High resolution group velocity analysis. *Geoexploration*, 16(1–2), 97–109. [https://doi.org/10.1016/0016-7142\(78\)90009-1](https://doi.org/10.1016/0016-7142(78)90009-1)
- Molenaar, C. M., & Halverson, D. V. (1969). Nomenclature chart of the Grand Canyon and adjacent areas. In *Geology and natural history of the grand canyon region: Four corners geological society guidebook, fifth field conference* (pp. 68–77).
- Nyberg, B., Nixon, C. W., & Sanderson, D. J. (2018). NetworkGT: A GIS tool for geometric and topological analysis of two-dimensional fracture networks. *Geosphere*, 14(4), 1618–1634. <https://doi.org/10.1130/GES01595.1>
- Pollack, H. N., & Chapman, D. S. (1977). Mantle heat flow. *Earth and Planetary Science Letters*, 34(2), 174–184. [https://doi.org/10.1016/0012-821x\(77\)90002-4](https://doi.org/10.1016/0012-821x(77)90002-4)
- Prodehl, C., & Pakiser, L. C. (1980). Crustal structure of the southern Rocky Mountains from seismic measurements. *Bulletin of the Geological Society of America*, 91(3), 147–155. [https://doi.org/10.1130/0016-7606\(1980\)91<147:csotsr>2.0.co;2](https://doi.org/10.1130/0016-7606(1980)91<147:csotsr>2.0.co;2)
- Roller, J. C. (1965). Crustal structure in the eastern Colorado Plateau Province from seismic refraction measurements. *Bulletin of the Seismological Society of America*, 55(1), 107–119.
- Ryaboy, V., Baumgardt, D. R., Firbas, P., & Dainty, A. M. (2001). Application of 3-D crustal and upper mantle velocity model of North America for location of regional seismic events. *Pure and Applied Geophysics*, 158(1–2), 79–103. <https://doi.org/10.1007/pl00001169>
- Sheehan, A. F., Abers, G. A., Jones, C. H., & Lerner-Lam, A. L. (1995). Crustal thickness variations across the Colorado Rocky Mountains from teleseismic receiver functions. *Journal of Geophysical Research*, 100(B10), 20391–20404. <https://doi.org/10.1029/95jb01966>
- Shen, W., Ritzwoller, M. H., & Schulte-Pelkum, V. (2013). A 3-D model of the crust and uppermost mantle beneath the Central and Western US by joint inversion of receiver functions and surface wave dispersion. *Journal of Geophysical Research, Solid Earth*, 118(1), 262–276. <https://doi.org/10.1029/2012jb009602>
- Slack, P. D., Davis, P. M., Baldrige, W. S., Olsen, K. H., Glahn, A., Achauer, U., & Spence, W. (1996). The upper mantle structure of the central Rio Grande rift region from teleseismic P and S wave travel time delays and attenuation. *Journal of Geophysical Research*, 101(B7), 16003–16023. <https://doi.org/10.1029/96jb00109>
- Snelson, C. M., Henstock, T. J., Keller, G. R., Miller, K. C., & Levander, A. (1998). Crustal and uppermost mantle structure along the Deep Probe seismic profile. *Rocky Mountain Geology*, 33(2), 181–198. <https://doi.org/10.2113/33.2.181>
- SMU Node of National Geothermal Data System. (2022). SMU Borehole temperature (BHT) database. Retrieved from <http://geothermal.smu.edu/gtda/>
- Spencer, C. W. (1978a). Tooto dome Pennsylvanian “D” (oil), T. 26 N., R. 18 W., NMPM, san Juan County, New Mexico. In *Four corners geological society. Oil and gas fields of the four corners area* (Vol. I–II, pp. 522–527).
- Spencer, C. W. (1978b). Tohache wash area (helium), T. 41 N., R. 30 E., GandSRM, Apache County, Arizona. In *Four Corners geological society. Oil and gas fields of the four corners area* (Vol. III, pp. 92–93).
- Stankova, J., Bilek, S. L., Rowe, C. A., & Aster, R. C. (2008). Characteristics of the October 2005 microearthquake swarms over decadal time periods near Socorro, New Mexico. *Bulletin of the Seismological Society of America*, 98(1), 93–105. <https://doi.org/10.1785/0120070108>
- Steinhart, J. S. & Meyer, R. P. (Eds.) (1961). *Explosion studies of continental structure* (Vol. 622, pp. 226–383). University of Wisconsin, Carnegie Institution of Washington
- Topozada, T. R., & Sanford, A. R. (1976). Crustal structure in central New Mexico interpreted from the Gasbuggy explosion. *Bulletin of the Seismological Society of America*, 66(3), 877–886. <https://doi.org/10.1785/bssa0660030877>
- University of Delaware Terrestrial Precipitation. (2018). Version 5.01, NetCDF4, ASCII, NOAA ESRL. Retrieved from https://www.esrl.noaa.gov/psd/data/gridded/data.UDel_AirT_Precip.html
- Warren, D. H. (1969). A seismic-refraction survey of crustal structure in central Arizona. *Geological Society of America Bulletin*, 80(2), 257–282. [https://doi.org/10.1130/0016-7606\(1969\)80\[257:assoc\]2.0.co;2](https://doi.org/10.1130/0016-7606(1969)80[257:assoc]2.0.co;2)